Organic Electronics 13 (2012) 361–365

Contents lists available at SciVerse ScienceDirect

Organic Electronics

journal homepage: www.elsevier.com/locate/orgel

Mapping the built-in electric field in polymer light-emitting electrochemical cells

Yufeng Hu [a], Bryce Dorin [a], Feng Teng [b], Jun Gao [a,*]

[a] Department of Physics, Queen's University, Kingston, Ontario, Canada K7L 3N6
[b] Key Laboratory of Luminescence and Optical Information, Ministry of Education, Institute of Optoelectronic Technology, Beijing Jiaotong University, Beijing 100044, China

ARTICLE INFO

Article history:
Received 19 October 2011
Received in revised form 8 December 2011
Accepted 11 December 2011
Available online 2 January 2012

Keywords:
Polymer light-emitting electrochemical cells
p–n Junction
Built-in electric field
Electrochemical doping

ABSTRACT

A millimeter planar polymer light-emitting electrochemical cell was turned on in a cryogenic probe station and subsequently cooled to freeze the doping profile. A 442 nm laser beam guided by an optical fiber was scanned across the interelectrode gap of several millimeters and the photovoltaic response was measured as a function of position. Both photocurrent and photovoltage profiles display a prominent peak at the geometric boundary of the p- and n-doped regions. A non-zero photovoltaic response throughout the p- and n-doped regions can be explained by various broadening mechanisms including non-uniform doping and secondary excitation by waveguided light. The photovoltaic response is weakest at the electrode/polymer interfaces.

1. Introduction

Polymer light-emitting electrochemical cells (LECs) have been the subject of numerous recent studies all aimed at understanding the complex operating mechanisms of these devices [1–5]. LECs are unique among organic devices in that their active layer is a mixed ionic–electronic conductor consisting of a luminescent conjugated polymer and a solid-state polymer electrolyte [6]. The luminescent polymer is electrochemically p- and n-doped *in situ* via the application of a voltage bias. A light-emitting p–n junction is formed when the doped regions expand and make contact. The dynamic LEC doping process has been visualized by time-lapse fluorescence imaging of planar cells with an extremely large interelectrode gap [7,8]. The electronic structure of the LEC p–n junction, however, has not yet been adequately characterized.

LECs in a planar configuration have an exposed and highly scalable interelectrode gap that can be easily accessed both optically and electrically. Pingree et al. applied scanning Kelvin probe microscopy (SKPM) to measure the potential profiles of μm-gap planar LECs under bias [9]. By varying the electrolyte salt and electrode materials, the group was able to shift the junction position and observe potential profiles well correlated with the optically imaged junction position [10]. The SKPM study by Matyba et al. on 120 μm planar LECs shows that the steepest potential drop occurs about 35 μm away from the cathode interface which is again consistent with the junction position [11]. Our group pioneered the turn-on and fluorescence imaging of planar LECs with millimeter interelectrode spacing [12]. The extremely large planar cells offer ease of fabrication and allow flexible testing schemes. For potential mapping, a 10.4 mm-planar LEC was turned on in a cryogenic probe station and promptly cooled to 200 K to freeze the doping profile. The potential drop due to an applied constant current was measured using a micro-manipulated tungsten probe in direct contact with the polymer film. The results establish that the doping profile of the planar LEC is that of a graded p–n junction. The doped polymer film is highly conductive and the p-doped region is more conductive than the n-doped region [13].

* Corresponding author.
E-mail address: jungao@physics.queensu.ca (J. Gao).

1566-1199/$ - see front matter © 2011 Elsevier B.V. All rights reserved.
doi:10.1016/j.orgel.2011.12.010

Since an LEC once turned on is a p–n junction, it also possesses a built-in potential due to the chemical potential difference of the p- and n-doped polymers. Large, electrode-independent LEC built-in potential manifested as photovoltage has been observed in both sandwich and planar frozen-junction LECs under illumination [14,15]. LEC built-in potential is also responsible for the large open-circuit voltage observed when a fully charged sandwich cell is allowed to relax at room temperature [16]. In a planar cell configuration, the built-in potential could be spatially resolved using SKPM scans to show that it had indeed originated from the relaxing p–n junction [11]. For stable doping profiles, the optical-beam-induced-current (OBIC) technique is widely used to map the built-in potential or built-in electric field [17,18]. In OBIC measurements a focused light beam is scanned across the device and the photocurrent is detected whose magnitude is proportional to the strength of the local built-in electric field. The OBIC technique has been used to map the built-in potential of a 20 μm-planar LEC with a focused Ar ion laser beam [19]. Open-circuit voltage was detected in a narrow region (~2 μm wide) that was identified as the location of the p–n junction. Additionally, the photovoltage increased with the voltage bias that was applied to turn on the device. These results are consistent with the LEC operating mechanism by electrochemical doping and p–n junction formation. However, this initial LEC OBIC study preceded the discovery of frozen-junction LECs. The planar LEC was only cooled to 250 K after turn-on, which is above the glass transition temperature of polyethylene oxide (PEO)–lithium triflate electrolyte. We have shown that at 250 K the junction is not sufficiently frozen [20]. This and the low excitation power used (nW) are likely responsible for the extremely weak (microvolt) photovoltage detected. Photocurrent was not measured to avoid rapid junction relaxation under short-circuit conditions. Here we present OBIC study of mm-gap planar LECs frozen at 200 K. Both photovoltage and photocurrent scans have been carried out along with photoluminescence and electroluminescence imaging of the device.

The planar LECs used in this study contained MEH-PPV, PEO (molecular weight 100 k) and cesium perchlorate ($CsClO_4$) in a weight ratio of 10:10:3. PEO and $CsClO_4$ were purchased from Aldrich and used as received. The LEC film was spin cast from a cyclohexanone solution and had thickness of 335 ± 6 nm, as determined with an optical profiler. Co-planar gold and aluminum electrodes were evaporated on top of the LEC film using two sets of shadow masks in two steps. This involved the breaking of vacuum to switch the shadow masks for the second evaporation. The gold strip electrode has variable width so that each LEC has two interelectrode gaps of 3.1 mm and 4.6 mm, respectively. The cell was mounted in a Janis ST-500-1 micromanipulated cryogenic probe station for testing under vacuum (~10^{-5} torr). Electrical contact to the device was made via two tungsten probes maneuvered by independent X–Y–Z translation stages. Tiny indium balls were attached to the tips of the probe to ensure good electrical contact to the

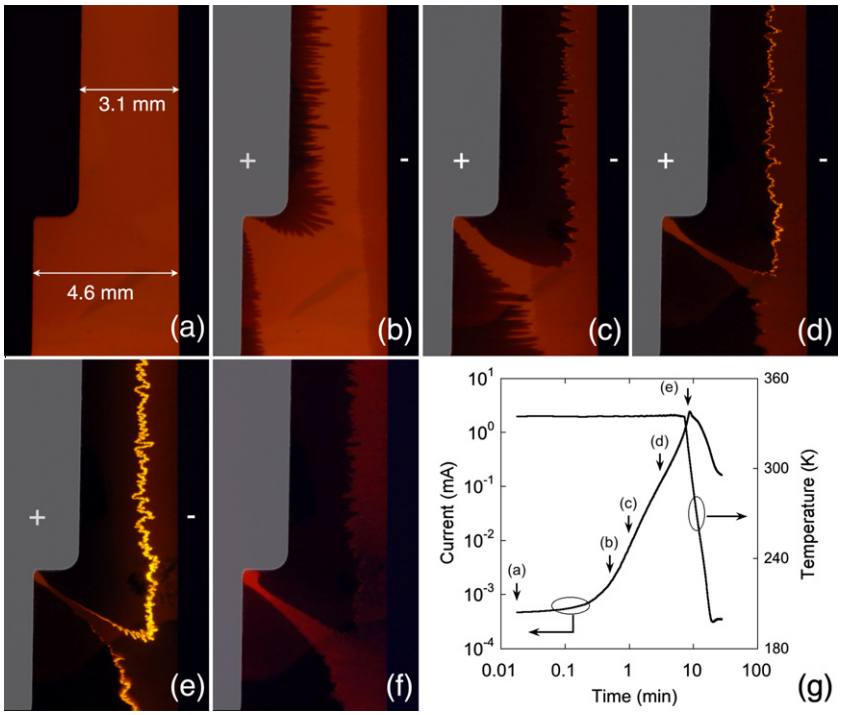

Fig. 1. Time-lapse fluorescence imaging of a MEH-PPV:PEO:$CsClO_4$ planar LEC with variable interelectrode spacing. The device was under 365 nm UV illumination and initially held at 335 K. The images were taken (a) 0 min, (b) 0.5 min, (c) 1 min and (d) 3 min after a 300 V bias was applied. Image (e) was taken at t = 8 min during cool down and at approximately 320 K. Image (f) shows the stabilized doping profile at 200 K without bias. (g) The cell current and temperature as a function of time during the turn on/cool down process. In (b–f) the gold electrode is highlighted for visibility. (For interpretation of the references to colour in this figure legend, the reader is referred to the web version of this article.)

electrodes. Another X–Y–Z translational stage holds an optical fiber coupled to a Melles Griot helium–cadmium laser to provide localized optical excitation of 4 mW (output from fiber tip) at 442 nm. The multimode, step-index optical fiber was positioned just above the surface of the film. We therefore approximate the beam size as that of the optical fiber core diameter (200 μm).

The planar cell was turned on by applying a 300 V bias to the gold electrode with respect to the aluminum electrode. Under ultraviolet illumination, strong PL quenching induced by electrochemical p- and n-doping was highly visible (Fig. 1a and b). When the progressing doping fronts made contact a light-emitting p–n junction was formed (Fig. 1c). Afterwards doping level continued to increase as the doped regions darkened. This led to a sharp increase in device current and junction electroluminescence (Fig. 1d and e). The wider part of the device had slower doping propagation due to lower electric field and higher resistance. But eventually both 3.1 and 4.6 mm parts of the device turned on and exhibited strong junction electroluminescence. A doping free region remained where the local electric field is the weakest due to the positive curvature of the gold electrode. Cooling of the device began when the device current reached 1 mA. The device had very good thermal contact to the cooling stage due to the use of silver-based thermal paste between the thin sapphire substrate (~1 mm) and the gold plated sample stage, but the current still overshot to about 3 mA before responding to the temperature drop. The frozen doping profile at 200 K can be seen in Fig. 1f, which is drastically different from Fig. 1a before the voltage bias was applied. The sharp transition region between the darker p-doped region and the lighter n-doped regions is the location of the geometric p–n junction.

With the LEC frozen at 200 K and the initial voltage bias removed, OBIC scans were carried out to map the built-in electric field along several paths. The optical fiber was manually scanned edge-to-edge from the Al electrode to the Au electrode with a 50 μm step size. A Keithley 237 source measurement unit held the device at 0 V and simultaneously measured the photocurrent (i.e. short-circuit current). The optical fiber was then moved back to the starting point and the photovoltage (open-circuit voltage) was measured while maintaining zero cell current. Fig. 2 shows the photocurrent/photovoltage profile for the scan path shown at the top. In a p–n junction the built-in electric field points from n to p, as a result we observe a negative photocurrent (flowing from Au to A1 electrode externally) and a positive photovoltage. In addition, the peak photocurrent and photovoltage signals occur precisely at the location of the geometric p–n junction where the built-in electric field is the strongest. The peak photovoltage in Fig. 2 is over 0.6 V, which is quite high considering the p–n junction formed has not been relaxed and is quite "leaky" due to the large tunneling current under reverse bias [15]. In addition, it is known that the photovoltage is lowered by local illumination due to the large dark cell in parallel to the small illuminated area [21].

We note that the profiles in Fig. 2 are extremely wide. A Gaussian fit yields a FWHM of 0.46 mm for photocurrent and 0.82 mm for photovoltage, which are both much larger

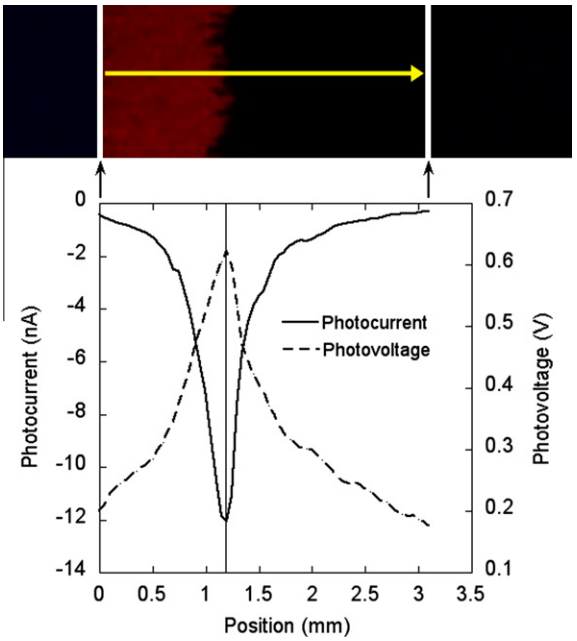

Fig. 2. OBIC photocurrent and photovoltage profiles of the frozen junction cell shown in Fig. 1 in the 3.1 mm spacing region. Top: portion of the cell under UV. The vertical white lines indicate the electrode/polymer film interfaces. The yellow line and arrow depict the scan path and direction. Bottom: photocurrent and photovoltage profiles for the scan path shown at the top. (For interpretation of the references to color in this figure legend, the reader is referred to the web version of this paper.)

than the beam diameter. The peak positions are about 1.19 mm from the Al electrode. Several factors could have contributed to the wide photocurrent and photovoltage profiles: (1) The p–n junction is not straight due to uneven doping propagation. (2) The doping concentration is non-uniform in the neutral p- and n-regions. A doping gradient is associated with a built-in electric field that can give rise to a non-zero OBIC signal. (3) The p–n junction is excited by waveguided and/or scattered light. While (1) will certainly have an effect on the OBIC profile near the junction, (2) and/or (3) must also be invoked in order to explain the non-zero OBIC signal far from the junction region. In fact, the baseline OBIC signal near the electrodes is most likely due to indirect excitation of the junction from scattered and reflected light as the signal did not diminish even when the laser spot is entirely on top of the electrode. Widening of the OBIC profile due to exciton diffusion to the junction region is unlikely since we are dealing with a millimeter length scale. We also observe that the photovoltage profile is consistently wider than the photocurrent profile. This is due to a logarithmic relation between voltage and current in a pn junction diode. As a result, photovoltage does not fall off as quickly as photocurrent.

A significant observation is the lack of OBIC response at both electrode interfaces, apart from an elevated baseline that can be attributed to excitation by scattered light. On the contrary, non-negligible potential drops have been observed at electrode interfaces in the mapping of micrometer planar LECs using scanning probe microscopic techniques

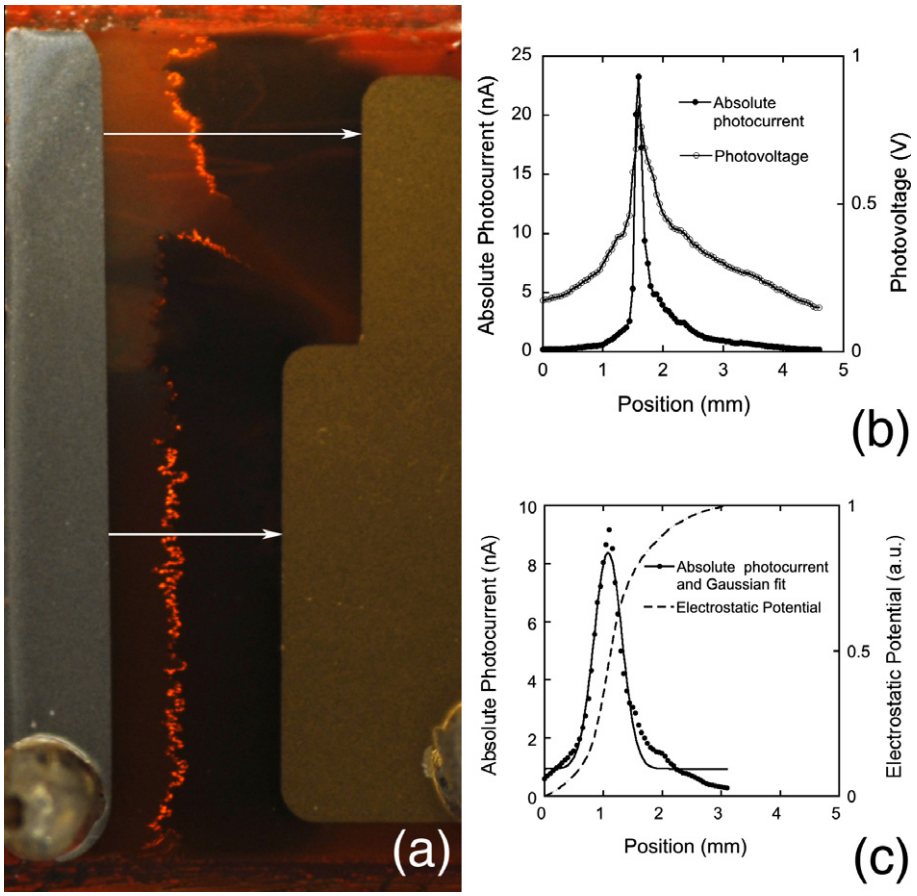

Fig. 3. Additional OBIC scans of the frozen junction cell shown in Fig. 1. (a) Global view of the frozen cell under 300 V bias at 200 K. Some room light was filled into reveal the aluminum and gold electrodes. The scan path and directions are shown as white lines and arrows. The 300 V bias was removed during the OBIC scans. (b) Photocurrent and photovoltage profiles of the 4.6 mm path. (c) Photocurrent profile and Gaussian fit of the 3.1 mm path. Also shown is the electrostatic potential profile generated by integrating the photocurrent profile. (For interpretation of the references to colour in this figure legend, the reader is referred to the web version of this article.)

[22,23]. The difference is likely the result of higher conductivity in our millimeter planar LECs. The high conductivity of our polymer film leads to ohmic contacts that are transparent to the OBIC technique due to the lack of a significant depletion region. In addition, optical absorption is diminished due to high doping levels near the electrodes.

Fig. 3a provides a view of the entire device *under bias* when it was frozen at 200 K. Some room light was filled in during the exposure to make the electrodes visible. We note that part of the device was no longer emitting due to degradation during the turn on process. Two additional paths were chosen for OBIC scans as indicated by the arrowed lines. Fig. 3b shows the (absolute) photocurrent and photovoltage profiles in the wider 4.6 mm region. The peak photocurrent is located 1.6 mm from the Al electrode, again reflecting the actual junction position. The much stronger peak signals indicate better junction quality in the wider region. The photocurrent profile is narrower than the photovoltage profile for the reason given above. We observe that the emitting junction crossing the scan path is much less jagged and nearly perpendicular to the scan direction. This is likely why the photocurrent profile is also narrower than in the 3.1 mm section of the device.

An interesting feature of photocurrent profile is its obvious asymmetry. The falloff on the n-side is much faster than on the p-side. Spectroscopic evidence shows that electrochemical doping in LECs reduce π–π^* absorption [16]. Since the heavily PL quenched p region is nearly transparent to the excitation beam, the OBIC tail is unlikely caused by local light absorption. A more probable cause is the excitation of the junction by waveguided light. The opposite is true on the n region where the absorption is significant and the doping gradient is the cause of less pronounced profile widening. The OBIC profile in Fig. 3c closely resembles the OBIC profile shown in Fig. 2 in peak position, FWHM and overall shape except for its slightly lower peak amplitude. The Gaussian fit shows large deviation in regions far from the pn junction. The electrostatic potential profile, obtained by integrating the OBIC profile, resembles that of a graded pn junction. However, since various broadening mechanisms have contributed to the broadening of the OBIC profile, the built-in potential profile should be interpreted with caution, especially on the p side of the junction.

In summary, we have carried out OBIC scans on a planar LEC with interelectrode gaps of 3.1 mm and 4.6 mm. The

cell was frozen at 200 K and scanned under both open-circuit and short-circuit conditions. The strong photovoltage and photocurrent signals support the existence of a significant built-in electric field. Aided by the concerted fluorescence and electroluminescence imaging of the same device, the peak OBIC signal is attributed to the polymer p–n junction formed by *in situ* electrochemical doping. The polymer/electrode interfaces are ohmic contacts and optically inactive. The width of the depletion region, however, is not extracted due to the large diameter of the excitation beam and the various profile-broadening mechanisms. The use of a focused beam and a more precise translational stage would make it possible to study the fine electronic structure of the static p–n junction.

Acknowledgements

This project is supported by a Discovery Grant from the Natural Sciences and Engineering Research Council of Canada. Feng Teng thanks financial support from Grant NSFC 61077022, China.

References

[1] K.O. Burnett, P.P. Crooker, N.M. Haegel, Y. Yoshioka, D. MacKenzie, Synthetic Metals 161 (15–16) (2011) 1496–1499.
[2] S. van Reenen, R.A.J. Janssen, M. Kemerink, Organic Electronics 12 (10) (2011) 1746–1753.
[3] S. van Reenen, P. Matyba, A. Dzwilewski, R.A.J. Janssen, L. Edman, M. Kemerink, Advanced Functional Materials 21 (10) (2011) 1795–1802.
[4] V. Bychkov, P. Matyba, V. Akkerman, M. Modestov, D. Valiev, G. Brodin, C.K. Law, M. Marklund, L. Edman, Physical Review Letters 107 (1) (2011) 016103.
[5] Z. Yu, M. Wang, G. Lei, J. Liu, L. Li, Q. Pei, Journal of Physical Chemistry Letters 2 (5) (2011) 367–372.
[6] Q.B. Pei, G. Yu, C. Zhang, Y. Yang, A.J. Heeger, Science 269 (5227) (1995) 1086–1088.
[7] J. Gao, J. Dane, Applied Physics Letters 84 (15) (2004) 2778–2780.
[8] Y.F. Hu, C. Tracy, J. Gao, Applied Physics Letters 88 (12) (2006) 123507.
[9] L.S.C. Pingree, D.B. Rodovsky, D.C. Coffey, G.P. Bartholomew, D.S. Ginger, Journal of the American Chemical Society 129 (51) (2007) 15903–15910.
[10] D.B. Rodovsky, O.G. Reid, L.S.C. Pingree, D.S. Ginger, ACS Nano 4 (5) (2010) 2673–2680.
[11] P. Matyba, K. Maturova, M. Kemerink, N.D. Robinson, L. Edman, Nature Materials 8 (8) (2009) 672–676.
[12] J. Gao, J. Dane, Applied Physics Letters 83 (15) (2003) 3027–3029.
[13] Y. Hu, J. Gao, Journal of the American Chemical Society 133 (7) (2011) 2227–2231.
[14] J. Gao, G. Yu, A.J. Heeger, Applied Physics Letters 71 (10) (1997) 1293–1295.
[15] Y. Zhang, Y. Hu, J. Gao, Applied Physics Letters 91 (23) (2007) 233509.
[16] Q.B. Pei, Y. Yang, G. Yu, C. Zhang, A.J. Heeger, Journal of the American Chemical Society 118 (16) (1996) 3922–3929.
[17] T. Wilson, C. Sheppard, Theory and Practice of Scanning Optical Microscopy, Academic Press, London, Orlando, 1984.
[18] D. Reuter, C. Werner, A.D. Wieck, S. Petrosyan, Applied Physics Letters 86 (16) (2005) 162110.
[19] D.J. Dick, A.J. Heeger, Y. Yang, Q.B. Pei, Advanced Materials 8 (12) (1996) 985–987.
[20] Y. Zhang, J. Gao, Journal of Applied Physics 100 (2006) 084501.
[21] A. Manor, E.A. Katz, R. Andriessen, Y. Galagan, Applied Physics Letters 99 (17) (2011) 173305.
[22] S. van Reenen, P. Matyba, A. Dzwilewski, R.A.J. Janssen, L. Edman, M. Kemerink, Journal of the American Chemical Society 132 (39) (2010) 13776–13781.
[23] J.D. Slinker, J.A. DeFranco, M.J. Jaquith, W.R. Silveira, Y.W. Zhong, J.M. Moran-Mirabal, H.G. Craighead, H.D. Abruna, J.A. Marohn, G.G. Malliaras, Nature Materials 6 (11) (2007) 894–899.